J. Fluid Mech. (1981), *vol.* 111, *pp.* 1–14
Printed in Great Britain

Two-layer rotating steady viscous flow over long ridges

By DON L. BOYER

Department of Mechanical Engineering,
University of Wyoming, Laramie

(Received 23 May 1979 and in revised form 11 December 1980)

The flow of a rotating, two-layer fluid system over long ridges of constant cross-section is considered. Homogeneous incompressible fluids of constant, but different, density are confined between two 'infinite' horizontal plane surfaces which rotate at a constant angular velocity about a vertical axis. The ridge is located on the lower surface while upstream of the ridge each fluid is in uniform motion in a direction normal to the ridge. Solutions are obtained for both an f-plane and a β-plane under the following restrictions: $E \ll 1$, $Ro \sim E^{\frac{1}{2}}$, $S \sim O(1)$, $H/L \sim O(1)$, $d/L \sim O(1)$ and $h/L \sim E^{\frac{1}{2}}$ where E is the Ekman number, Ro is the Rossby number, S is a stratification parameter, H/L is the two-fluid depth to ridge width ratio, d/L is the lower fluid depth to ridge width ratio and h/L is the aspect ratio of the ridge. This set of restrictions assures that viscosity is important in considering the dynamics of the system. Furthermore the restrictions are ones that make laboratory experimentation feasible. Solutions are also presented for the non-viscous case (i.e. $E = 0$), and are compared with their viscous counterparts. The importance of viscosity in this physical system is thus demonstrated.

1. Introduction

Since Taylor's (1923) pioneering experiments, much work has been done both theoretically and experimentally on the effect of various topographic features on the flow of rotating fluids. This work in general has been motivated by possible applications to 'real geophysical situations' such as atmospheric motions, ocean currents, and such matters as Hide's (1961) hypothesis concerning Jupiter's great red spot being a Taylor column. Much work remains to be done, however. As noted by Huppert (1975), 'Taylor's work has not been extended sufficiently, so that we do not yet know the solution to the relevant, purely theoretical problem; that is, the form of motion to be expected in an arbitrarily stratified, slightly viscous shear flow over prescribed topography in a rapidly rotating system incorporating the β-effect'.

A good summary of the theoretical work done on investigating topographic effects in rotating flows (i.e. Taylor columns and related phenomena) is given by McCartney (1975). As noted in that paper, theoreticians must in general neglect various parameters (e.g. inertia, viscosity, stratification, or the β-effect) or make restrictive assumptions on others (e.g. infinitesimal topographic features) so that a tractable set of governing equations can be realized. These restrictions generally limit the usefulness of the results in applications to 'real geophysical flows' as well as making laboratory experimentation concerning the stated problem, in most cases, difficult, if not impossible.

In a series of papers by Boyer (1971*a*, *b*) and Vaziri & Boyer (1971), the flow of a single layer fluid on an f-plane was investigated both theoretically and by laboratory

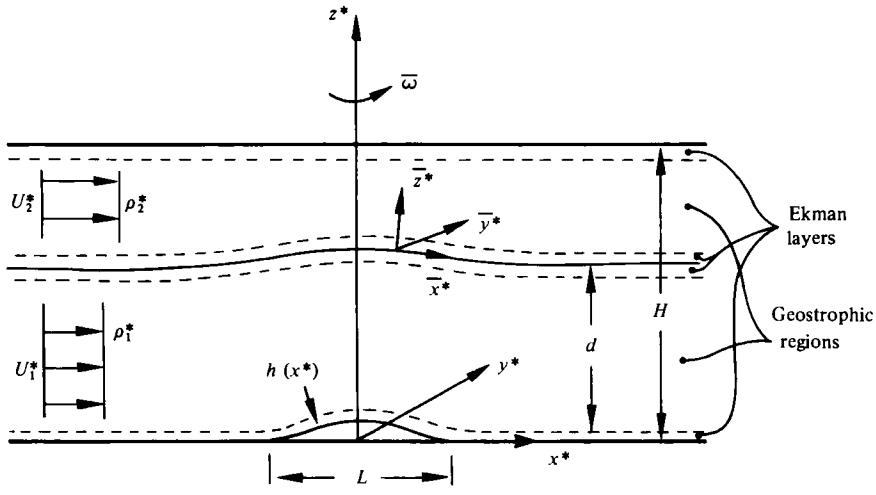

FIGURE 1. Physical system.

experiment for a range of dimensionless parameters for which theory and experiment coincided and for which inertia, viscosity, and Coriolis effects were included; the aspect ratio of the topographic features was taken as infinitesimal and stratification was not considered. This work was later extended to include the β-effect; Vaziri & Boyer (1977). In all of these studies there was good agreement between the experiments and the theory advanced.

The purpose of the present paper is to extend the earlier work to a two-layer model and to provide an analysis which will be applicable for a range of parameters which can be examined in the laboratory. In essence it is an extension of the theoretical system considered by McCartney (1975) but includes the effect of viscosity, which is an important consideration for laboratory experimentation. We will restrict to the flow over a long ridge of constant cross-section because the analytical simplifications so made allow for closed-form solutions.

The physical system to be considered is given in figure 1. Two layers, each of uniform but different density (ρ_1^*, ρ_2^*) are confined between two infinite, plane horizontal surfaces which are rotating with an angular velocity, $\omega\hat{k}$, about a vertical axis. Each layer is taken to be in uniform rectilinear motion with speed U_1^* and U_2^* relative to a rotating observer. In § 3, the β-plane situation is discussed; the bounding surfaces are then taken as tilted in the north, south $(+y^*, -y^*)$ directions. A low-aspect-ratio ridge of profile $h(x^*)$ is located on the lower plane surface. The streamwise extent of the ridge is given by L, the depth of the lower fluid, by d, and that of the upper fluid, by $H-d$. It is desired to determine the resulting flow field.

For the range of parameters considered, each fluid has an interior geostrophic region. Ekman boundary layers exist along the bounding surfaces, as well as in each fluid along the interface between the fluids. The lowest-order solution is obtained by considering asymptotic expansions of the velocity and pressure fields in $E^{\frac{1}{2}}$ in each of these regions, where E is the Ekman number, and then matching the terms appropriately at the various boundaries. Inviscid solutions are also obtained to compare with the viscous results.

In § 2 solutions for the f-plane are developed. In § 3 the analysis is extended to the

β-plane with solutions for retrograde (westward) and prograde (eastward) flow being discussed. Some concluding remarks are made in § 4.

2. f-plane

Consider each layer of a two-layer flow to be a homogeneous incompressible fluid in steady-state motion relative to a rectangular Cartesian co-ordinate system $\bar{x}^*(x^*, y^*, z^*)$ rotating at an angular velocity $\omega\hat{k}$ with respect to an inertial frame; see figure 1. The equations of motion are given by

$$(\bar{v}_i^* . \nabla_*)\,\bar{v}^* = -\frac{1}{\rho_i^*}\nabla_* p_i^* - g\hat{k} - 2\omega(\hat{k}\times\bar{v}_i^*) + \nu\nabla_*^2\,\bar{v}_i^* \tag{2.1}$$

and

$$\nabla_* . \bar{v}_i^* = 0, \tag{2.2}$$

where $i = 1$ (lower layer) and $i = 2$ (upper layer); $\bar{v}^*(u^*, v^*, w^*)$ is the Eulerian velocity; ρ^* the density; p^* the pressure; g the acceleration of gravity; and ν the kinematic viscosity (assumed equal in each layer). For fluids of different viscosities this last restriction can easily be relaxed. Relations (2.1) and (2.2) correspond, respectively, to conservation of momentum and mass. In order to develop a tractable theory, centrifugal effects are neglected *a priori*. This restriction may cause difficulty in applying the theory to laboratory experiments.

We now introduce the following dimensionless parameters:

$$\left.\begin{aligned} &\bar{x}_i = \frac{\bar{x}_i^*}{L}, \quad \bar{v}_i = \frac{\bar{v}_i^*}{U_0^*}, \quad \rho_i = \frac{\rho_i^*}{\rho_0^*}, \\ &\Phi_1 = \{p_1^* - \rho_2^* g(H-d) - \rho_1^* g(d-z^*)\}/2\omega\rho_1^* U_0^* L, \\ &\Phi_2 = \{p_2^* - \rho_2^* g(H-z^*)\}/2\omega\rho_2^* U_0^* L; \end{aligned}\right\} \tag{2.3}$$

where

$$U_0^* = \frac{dU_1^* + (H-d)\,U_2^*}{H}$$

and

$$\rho_0^* = \frac{d\rho_1^* + (H-d)\,\rho_2^*}{H}$$

are the average free-stream velocity and density, respectively; and where the remaining terms are defined in figure 1. Substituting these relations into (2.1) and (2.2) yields

$$Ro(\bar{v}_i . \nabla)\,\bar{v}_i = -\nabla\Phi_i - \hat{k}\times\bar{v}_i + E\nabla^2\bar{v}_i \tag{2.4}$$

and

$$\nabla . \bar{v}_i = 0 \tag{2.5}$$

respectively where $Ro = U_0^*/2\omega L$ is the Rossby number and $E = \nu/2\omega L^2$ is the Ekman number.

The boundary conditions on (2.4) and (2.5) are as follows:

(i) On the solid bounding surfaces we require no-slip; i.e.

$$\bar{v}_1(x, y, h(xL)/L) = 0, \quad \bar{v}_2(x, y, H/L) = 0.$$

(ii) Along the liquid–liquid interface we require continuity of velocity, pressure and shear stress; i.e.

$$\bar{v}_1 = \bar{v}_2, \quad p_1^* = p_2^*, \quad \bar{v}_{1\bar{z}} = \bar{v}_{2\bar{z}}$$

(see (2.3)), where $\bar{z}$ is the normal co-ordinate to the interface as shown in figure 1.

(iii) Far upstream and downstream of the topographic feature and outside the Ekman layers on the solid bounding surfaces and the fluid–fluid interface (for the range of parameter restrictions discussed below), we require:

$$\bar{v}_1(x \to -\infty, y, z) \to U_1 \hat{\imath}, \quad \bar{v}_2(x \to -\infty, y, z) \to U_2 \hat{\imath},$$

$$\bar{v}_{1x}(x \to \infty, y, z) \to 0, \quad \bar{v}_{2x}(x \to \infty, y, z) \to 0,$$

where $U_1 = U_1^*/U_0^*$ and $U_2 = U_2^*/U_0^*$.

The dynamic boundary condition at the interface between the fluids introduces a stratification parameter $S = g\Delta\rho^*/4\omega^2\rho_0^* L$ where $\Delta\rho^* = \rho_2^* - \rho_1^*$ is the density difference between layers. The problem as posed is thus a six-parameter one including Ro, E, S, H/L, d/L and h/L, where the last three are geometrical terms defined in figure 1.

We now consider the following *a priori* restrictions which are guided by the aim of investigating the physical system over a range of parameters which might be examined by laboratory experimentation: (i) $E \ll 1$; (ii) $Ro = kE^{\frac{1}{2}}$ where $k \sim O(1)$; (iii) $S \sim O(1)$; (iv) $H/L \sim O(1)$; (v) $d/L \sim O(1)$; and $h(xL)/L \sim O(E^{\frac{1}{2}})$. We write the last restriction for the topography as

$$h(xL)/L = E^{\frac{1}{2}} h_0(x), \tag{2.6}$$

where $h_0(x) \sim O(1)$. We also restrict to $h_{0x} \sim O(1)$; i.e. the topography is smooth. Under these restrictions the inertial, Coriolis, topographic, stratification, and viscous effects are all important in determining the lowest order motion.

As noted earlier, we will consider topographic features that are long ridges of constant cross-section and thus we take the velocity field to be independent of the co-ordinate along the ridge axis (i.e. $\bar{v}_y = 0$); note that the reduced pressures, Φ_1 and Φ_2, will be dependent on y. This leads to a linearization of the inertial terms and thus effects a substantial simplification of the analysis.

Let us first write the governing equations for the lower layer. Considering the deviation from uniform flow to be driven by Ekman layers along the bounding surfaces and the fluid–fluid interface, we assume that the dependent variables can be expanded in power series in $E^{\frac{1}{2}}$; i.e.

$$\left.\begin{aligned} u_1 &= f_0(x,z)\,E^0 + f_1(x,z)\,E^{\frac{1}{2}} + \ldots, \\ v_1 &= g_0(x,z)\,E^0 + g_1(x,z)\,E^{\frac{1}{2}} + \ldots, \\ w_1 &= l_0(x,z)\,E^0 + l_1(x,z)\,E^{\frac{1}{2}} + \ldots, \\ \Phi_1 &= m_0(x,y,z)\,E^0 + m_1(x,y,z)\,E^{\frac{1}{2}} + \ldots, \end{aligned}\right\} \tag{2.7}$$

where $f_0, \ldots, m_1, \ldots$ are assumed of order unity and where the leading terms are dictated by the order of the free-stream flow.

Substituting (2.7) into (2.4) and (2.5) one obtains the following zeroth-order equations:

$$m_{0x} = g_0, \quad m_{0y} = -f_0, \quad m_{0z} = 0, \quad f_{0x} + l_{0z} = 0 \tag{2.8}$$

respectively. Solving (2.8) subject to the condition $\bar{v} = U_1\hat{\imath}$ at $x \to -\infty$ we obtain

$$f_0 = U_1, \quad g_0 = g_0(x), \quad l_0 = 0, \quad m_0 = -U_1 y + \int g_0 dx. \tag{2.9}$$

In order to determine $g_0(x)$ it is necessary to consider the first-order equations; from (2.4), (2.5), (2.7) and (2.9) these are

$$m_{1x} = g_1, \quad kU_1 g_{0x} = -m_{1y} - f_1, \tag{2.10a, b}$$

$$m_{1z} = 0, \quad f_{1x} + l_{1z} = 0. \tag{2.10c, d}$$

Cross-differentiating the (2.10a, b), substituting the resulting value of f_{1x} into (2.10d) and integrating with respect to z, one obtains

$$l_1 = kU_1 z g_{0xx} + \alpha(x), \tag{2.11}$$

where $\alpha(x)$ is to be determined. From a consideration of the Ekman layers along the lower bounding surface it is then easy to show that the matching condition along $z = 0$ for the interior is given by

$$l_1(z=0) = U_1 h_{0x} + \frac{1}{\sqrt{2}} g_{0x}, \tag{2.12}$$

where the first term on the right is the vertical velocity due to the horizontal flow being turned by the topographic feature, and the second term is the contribution of Ekman suction. Equating (2.11), evaluated at $z = 0$, with (2.12), one can calculate $\alpha(x)$ and thus from (2.11) one obtains

$$l_1 = kU_1 z g_{0xx} + \frac{1}{\sqrt{2}} g_{0x} + U_1 h_{0x}. \tag{2.13}$$

This is the lowest-order vertical velocity component in the interior of the lower layer.

We now consider the interior solution in the upper layer. A power series similar to (2.7) is again assumed with a tilde used to designate an upper-layer dependent variable (e.g. $\tilde{g}_0$ is the lowest-order velocity component in the y direction in the upper layer). This analysis leads to the following zeroth-order solution (i.e. corresponding to (2.9) for the lower layer)

$$\tilde{f}_0 = U_2, \quad \tilde{g}_0 = \tilde{g}_0(x), \quad \tilde{l}_0 = 0, \quad \tilde{m}_0 = -U_2 y + \int \tilde{g}_0 dx, \tag{2.14}$$

where $\tilde{g}_0(x)$ is to be determined. As for the lower layer, the solution for $\tilde{g}_0(x)$ requires a consideration of the first-order equations. Writing these first-order relations and recognizing that the Ekman-boundary-layer matching condition at the upper surface is

$$\tilde{l}_1\left(z = \frac{H}{L}\right) = -\frac{1}{\sqrt{2}} \tilde{g}_{0x},$$

one obtains the following relation for the lowest-order vertical velocity component in the upper layer

$$\tilde{l}_1 = kU_2\left(z - \frac{H}{L}\right)\tilde{g}_{0xx} - \frac{1}{\sqrt{2}}\tilde{g}_{0x}. \tag{2.15}$$

To determine $g_0(x)$ and $\tilde{g}_0(x)$, and hence $l_1(x,z)$ and $\tilde{l}_1(x,z)$ from (2.13) and (2.15) respectively, we must now examine the boundary conditions along the interface

between the two fluids. The first condition requires the pressure to be continuous across the interface. Setting $p_1^* = p_2^*$ in (2.3) we obtain

$$\eta = \frac{R_0}{S}(\rho_1 \Phi_1 - \rho_2 \Phi_2) = \eta_0 E^{\frac{1}{2}}, \tag{2.16}$$

where η is the displacement of the interface from its non-rotating equilibrium position, and where η_0 is of order unity. Note from the parameter restrictions being considered (i.e. $Ro \sim E^{\frac{1}{2}}$ and $S \sim O(1)$), that η is of order $E^{\frac{1}{2}}$; η_0 is defined by (2.16).

Having retained the viscosity in the present formulation, the velocity and shear stress must also be continuous across the interface. Because the difference in the horizontal velocity field in the lower and upper geostrophic regions is in general of order unity, and because the elevation of the interface, η, is of order $E^{\frac{1}{2}}$, we assume that these velocity and shear stress conditions are satisfied by Ekman boundary layers along the interface in each of the fluids, respectively. To investigate these layers we introduce a local co-ordinate system $(\bar{x}, \bar{y}, \bar{z})$ along the interface where $\bar{x}$ is measured along the arc length formed by the intersection of the interface and the plane surfaces perpendicular to the y axis; $\bar{z}$ is normal to the interface; and $\bar{y}$ is chosen in the tangent plane so as to form a right-handed co-ordinate system (see figure 1).

Consider first the upper interfacial Ekman layer, and introduce the stretched boundary-layer co-ordinate $\zeta^+ = E^{-\frac{1}{2}}\bar{z}$. The lowest-order Ekman-layer equations from (2.4) and (2.5) are

$$\left.\begin{aligned} 0 &= -\tilde{g}_0(x) + v_{2\mathrm{E}} + u_{2\mathrm{E}\zeta^+\zeta^+}, \\ 0 &= U_2 - u_{2\mathrm{E}} + v_{2\mathrm{E}\zeta^+\zeta^+}, \\ u_{2\mathrm{E}x} &+ w_{2\mathrm{E}\zeta^+} = 0, \end{aligned}\right\} \tag{2.17}$$

where the subscript E represents an Ekman-layer variable; where the matching conditions with the upper layer have been satisfied; and where, with $\eta \sim O(E^{\frac{1}{2}})$, to lowest order $\bar{x} = x$ and $\bar{y} = y$.

Solving the first two of (2.17) we obtain

$$\left.\begin{aligned} u_{2\mathrm{E}} &= U_2 + [A^+ \cos(\zeta^+/\sqrt{2}) + B^+ \sin(\zeta^+/\sqrt{2})]\, e^{-\zeta^+/\sqrt{2}}, \\ v_{2\mathrm{E}} &= \tilde{g}_0(x) + [B^+ \cos(\zeta^+/\sqrt{2}) - A^+ \sin(\zeta^+/\sqrt{2})]\, e^{-\zeta^+/\sqrt{2}}, \end{aligned}\right\} \tag{2.18}$$

where A^+ and B^+ are to be determined.

A similar calculation for the lower Ekman layer, with $\zeta^- = -E^{-\frac{1}{2}}\bar{z}$, leads to

$$\left.\begin{aligned} u_{1\mathrm{E}} &= U_1 + [A^- \cos(\zeta^-/\sqrt{2}) + B^- \sin(\zeta^-/\sqrt{2})]\, e^{-\zeta^-/\sqrt{2}}, \\ v_{1\mathrm{E}} &= g_0(x) + [B^- \cos(\zeta^-/\sqrt{2}) - A^- \sin(\zeta^-/\sqrt{2})]\, e^{-\zeta^-/\sqrt{2}}, \end{aligned}\right\} \tag{2.19}$$

where A^- and B^- also are to be determined.

We now require that the velocity and shear stress be continuous across the interface between the fluids; i.e.

$$\left.\begin{aligned} u_{1\mathrm{E}}(\zeta^- = 0) &= u_{2\mathrm{E}}(\zeta^+ = 0), \quad v_{1\mathrm{E}}(\zeta^- = 0) = v_{2\mathrm{E}}(\zeta^+ = 0), \\ u_{1\mathrm{E}\zeta^-}(\zeta^- = 0) &= -u_{2\mathrm{E}\zeta^+}(\zeta^+ = 0), \quad v_{1\mathrm{E}\zeta^-}(\zeta^- = 0) = -v_{2\mathrm{E}\zeta^+}(\zeta^+ = 0). \end{aligned}\right\} \tag{2.20}$$

The integration constants in (2.18) and (2.19) are thus obtained by substituting these equations into the interface boundary conditions (2.20). The expression for $u_{2\mathrm{E}}$ in (2.18) is then substituted into the last of (2.17), the continuity relation for the Ekman layer, to determine the vertical velocity component, $w_{2\mathrm{E}}$, in the upper interfacial

Ekman layer; similarly w_{1E} is determined from the first of (2.19) and the corresponding continuity relation for the lower interfacial Ekman layer. We find

$$\left.\begin{aligned} w_{2E} &= -\frac{1}{2\sqrt{2}}(g_{0x}-\tilde{g}_{0x})\{1-[\cos(\zeta^+/\sqrt{2})+\sin(\zeta^+/\sqrt{2})]\,e^{-\zeta^+/\sqrt{2}}\},\\ w_{1E} &= -\frac{1}{2\sqrt{2}}(g_{0x}-\tilde{g}_{0x})\{1-[\cos(\zeta^-/\sqrt{2})+\sin(\zeta^-/\sqrt{2})]\,e^{-\zeta^-/\sqrt{2}}\},\end{aligned}\right\} \tag{2.21}$$

respectively. Letting $\zeta^+, \zeta^- \to \infty$, we thus note that the interfacial Ekman layers pump fluid into (or out of) the interior regions with a magnitude given by

$$w_{1E}(\zeta^- \to \infty) = w_{2E}(\zeta^+ \to \infty) = -\frac{1}{2\sqrt{2}}(g_{0x}-\tilde{g}_{0x}). \tag{2.22}$$

The interfacial matching condition for the interior flow in the upper and lower layers is thus composed of two parts. The first is the turning of the order one horizontal flow so that it is tangent to the interface. The second is the Ekman pumping contribution given by (2.22) where we note that, to lowest order, z and $\bar{z}$ are parallel. Using (2.16) and (2.22), the upper-layer interior matching condition is thus

$$\tilde{l}_1\left(z=\frac{d}{L}\right) = U_2\eta_{0x}+\tilde{g}_0\eta_{0y}-\frac{1}{2\sqrt{2}}(g_{0x}-\tilde{g}_{0x}). \tag{2.23}$$

Similarly, for the lower layer

$$l_1\left(z=\frac{d}{L}\right) = U_1\eta_{0x}+g_0\eta_{0y}-\frac{1}{2\sqrt{2}}(g_{0x}-\tilde{g}_{0x}). \tag{2.24}$$

From the last of relations (2.9) and (2.14), η_0 is determined from (2.16) as

$$\eta_0 = \frac{k}{S}\left\{-\rho_1 U_1 y+\rho_1\int g_0\,dx+\rho_2 U_2 y-\rho_2\int \tilde{g}_0\,dx\right\}. \tag{2.25}$$

Equating (2.13) evaluated at $z = d/L$ with (2.24) and utilizing (2.25); and equating (2.15) evaluated at $z = d/L$ with (2.23) and again utilizing (2.25), one obtains

$$g_{0xx}+a_0 g_{0x}+a_1 g_0+a_2\tilde{g}_{0x}+a_3\tilde{g}_0 = a_4 h_{0x}, \tag{2.26a}$$

$$\tilde{g}_{0xx}+b_0\tilde{g}_{0x}+b_1\tilde{g}_0+b_2 g_{0x}+b_3 g_0 = 0, \tag{2.26b}$$

respectively, where

$$a_0 = \frac{3L}{2\sqrt{2}kU_1 d},\quad a_1 = -\frac{U_2 L\rho_2}{U_1 dS},\quad a_2 = -\frac{L}{2\sqrt{2}kU_1 d},\quad a_3 = \frac{L\rho_2}{dS},\quad a_4 = -\frac{L}{kd};$$

$$b_0 = \frac{3L}{2\sqrt{2}kU_2(H-d)},\quad b_1 = -\frac{U_1 L\rho_1}{U_2(H-d)S},\quad b_2 = -\frac{L}{2\sqrt{2}kU_2(H-d)},\quad b_3 = \frac{L\rho_1}{(H-d)S}.$$

Relations (2.26) are the governing equations for g_0 and $\tilde{g}_0$ and are to be solved subject to the conditions

$$\left.\begin{aligned} &g_0(x),\quad \tilde{g}_0(x)\to 0 \quad \text{as} \quad x\to-\infty,\\ &g_{0x}(x),\quad \tilde{g}_{0x}(x)\to 0 \quad \text{as} \quad x\to\infty.\end{aligned}\right\} \tag{2.27}$$

With (2.13) and (2.15) then giving l_1 and $\tilde{l}_1$ respectively, the lowest-order solution is thus completed.

Depending on the choice of $h(xL)$, the coupled equations (2.26) can be solved subject to (2.27) in closed form by assuming exponential solutions or by using Fourier transforms. For complicated $h(xL)$, standard numerical solutions can also be employed.

One flow field characteristic of note for the f-plane case is that the interior streamlines are shifted laterally a finite distance from their upstream locations. Defining σ and $\tilde{\sigma}$ to be the respective shifts in the lower and upper layers we can write

$$\sigma = \frac{1}{U_1}\int_{-\infty}^{\infty} g_0(x)\,dx, \quad \tilde{\sigma} = \frac{1}{U_2}\int_{-\infty}^{\infty} \tilde{g}_0(x)\,dx. \tag{2.28}$$

By solving (2.26b) for g_0 and substituting this relation into (2.26a), integrating twice from $x = -\infty$ to $x = +\infty$, and then using (2.27), it can be shown that

$$\sigma = \tilde{\sigma} = 2\sqrt{2}\int_{-\infty}^{\infty} h_0 dx \Big/ \left[\frac{\rho_2}{\rho_1}\left(\frac{U_1 - 3U_2}{U_1}\right) + \left(\frac{U_2 - 3U_1}{U_1}\right)\right]. \tag{2.29}$$

Thus, the rather unexpected result that the streamline shift is the same for both layers. As in the earlier work of the writer (Boyer 1971a) the shift depends on the Ekman number (i.e. h_0 depends on E), but is again independent of the Rossby number. Presumably an analysis such as that given by Huppert & Stern (1974) for a channel with side walls would again give a dependence on Ro for the maximum streamline deflection.

To obtain a specific solution we consider the flow over a smooth symmetric ridge and assign values to the dimensionless parameters which might make laboratory experimentation feasible. In particular we define $U_1^* = U_2^* = U_0^* = 0{\cdot}2$ cm s^{-1}; $H = 5{\cdot}08$ cm; $d = 2{\cdot}54$ cm; $L = 5{\cdot}08$ cm; $h = 0{\cdot}254$ cm; $\omega = 1$ rad s^{-1}; $\rho_1^* = 1{\cdot}01$ gm cm^{-3}; $\rho_2^* = 1{\cdot}00$ gm cm^{-3}; $\nu = 0{\cdot}01$ cm^2 s^{-1}; and $g = 981$ cm s^{-2}. These give $E^{\frac{1}{2}} = 0{\cdot}014$, $Ro = 0{\cdot}020$, $S = 0{\cdot}48$, $H/L = 1{\cdot}0$, $d/L = 0{\cdot}5$ and $h/L = 0{\cdot}05$. We take the ridge topography in dimensionless form to be given by

$$h_0(x) = 3{\cdot}57\cos^2\pi x, \quad -0{\cdot}5 \leqslant x \leqslant 0{\cdot}5.$$

The solution of (2.26) subject to (2.27) for g_0 and $\tilde{g}_0$ can now be found in closed form in a straightforward way. The streamlines in the lower and upper layers are then given by

$$y = \frac{1}{U_1}\int_{-\infty}^{x} g_0(x)\,dx, \quad \tilde{y} = \frac{1}{U_2}\int_{-\infty}^{x} \tilde{g}_0(x)\,dx$$

respectively. The resulting horizontal streamline patterns for the lower and upper geostrophic regions are given in figure 2.

The qualitative aspects of the flow fields are similar to those obtained by Boyer (1971a) for the single-layer case. That is, in both layers the flow drifts to the right, facing downstream in the vicinity of the ridge and then returns to the same direction as the upstream flow, but shifted to the right, as discussed above. While the ridge had no effect on the upstream flow in the single-layer case, here the streamlines in both layers have some curvature upstream of the ridge.

In order to compare these 'viscous' results with those for the case in which viscosity is neglected (e.g. McCartney's analysis), an inviscid solution for the present problem was obtained. In the inviscid analysis the Ekman number, E, in (2.4) is identically zero. Solutions for the geostrophic regions are obtained by expanding the dependent

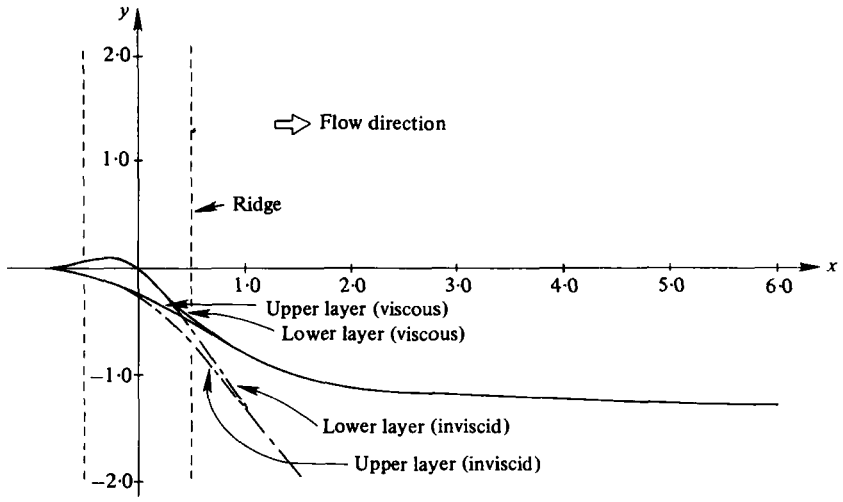

FIGURE 2. Streamline pattern for a cosine-squared ridge on an f-plane; $Ro = 0{\cdot}020$, $E = 1{\cdot}94 \times 10^{-4}$, $S = 0{\cdot}48$, $H/L = 1{\cdot}0$, $d/L = 0{\cdot}5$ and $h/L = 0{\cdot}05$. The free-stream velocity in each layer is the same; i.e. $U_1/U_2 = 1{\cdot}0$. Note, in the inviscid case $E = 0$.

variables in power series in the Rossby number, Ro. The matching conditions at the bounding surfaces are simply that the vertical velocity is zero along the top and is given by $RoU_1 h_{0x}$ along the bottom.

With zero viscosity, Ekman layers, of course, do not occur along the interface between the fluids. The boundary conditions along this interface are that the pressure is continuous (dynamic condition) and that the flow in each fluid layer is tangent to the interface (kinematic condition). The non-viscous analysis proceeds in a fashion almost identical to that given for the viscous case and is not repeated here. The resulting governing equations for the velocity components along the ridge are given by

$$g_{0xx} + a_1 g_0 + a_3 \tilde{g}_0 = a_4 h_{0x}, \quad \tilde{g}_{0xx} + b_1 \tilde{g}_0 + b_3 g_0 = 0, \tag{2.30}$$

where now

$$a_1 = -\frac{U_2 L \rho_2}{U_1 dS}, \quad a_3 = \frac{L\rho_2}{dS}, \quad a_4 = -\frac{L}{d};$$

$$b_1 = -\frac{U_1 L \rho_1}{U_2 (H-d) S}, \quad b_3 = \frac{L\rho_1}{(H-d)S};$$

and where $h_0(x) = (h(xL)/L)/Ro$. The solution of (2.30) is straightforward and for the same dimensional parameters (with $\nu = 0$) and ridge shape as given above gives the streamline pattern plotted in figure 2.

Hence, we see that in the inviscid case far downstream of the topography the velocity component parallel to the ridge is non-zero; the downstream flow direction thus differs from that upstream. From (2.30) it is easily shown that the downstream direction of the streamlines in each layer is given by

$$\tan\alpha = \frac{g_0(x \to \infty)}{U_1} = \frac{\tilde{g}_0(x \to \infty)}{U_2} = \frac{\rho_1 U_1 L \int_{-\frac{1}{2}}^{\frac{1}{2}} h_0(x)\, dx}{\rho_2 U_2^2 (H-d) + \rho_1 U_1^2 d}, \tag{2.31}$$

where α is the angle between the upstream and downstream streamlines (measured to the right facing downstream). Thus, we see that the effect of viscosity is to decay the relative vorticity generated by the topography and to return the streamlines to their original directions.

3. Beta-plane

In many applications to oceanographic or atmospheric motions the horizontal scale of the region in question is so large that the vertical component of the Earth's rotation varies substantially throughout the region. In such cases it has become customary to write the vertical component of the Earth's rotation as a Taylor series about the latitude of the central portion of the region being considered. The first term in such an expansion is called the β-term.

For single-layer studies it is possible to show that the β-effect can be simulated in the laboratory by simply tilting the fluid container from north to south with the 'thin' portion being toward the north; for example, see Greenspan (1968) and Vaziri & Boyer (1977). The latter study includes a solution for the flow of a single-layer fluid over a long ridge on a β-plane. A laboratory run is presented which is in good agreement with the theory. The question here is whether a tilting of the flow channel can simulate the β-effect for the two-layer case.

In examining this question we replace $2\bar{\omega}$ in relation (2.1) by

$$2\bar{\omega} = (2\omega_0 + \beta y)\hat{k}, \tag{3.1}$$

where in the simulation process, $2\omega_0$ is to represent twice the vertical component of the Earth's rotation rate at some central latitude; i.e. $2\Omega \sin \phi_0$ where Ω is the Earth's rotation rate and ϕ_0 is the latitude. The term β represents the first term in the Taylor expansion and is given by $2\Omega \cos \phi_0 / R$ where R is the Earth's radius and y is the co-ordinate measured toward the north.

If we now carry out the same non-dimensionalization as in (2.3) we find the Coriolis term in (2.4) is given by

$$\text{Coriolis term} = \left(1 + \frac{\beta L}{2\omega_0} y\right)(\hat{k} \times \bar{v}_i).$$

Thus, we have introduced a new dimensionless parameter $\beta L / 2\omega_0$. We take this quantity as being $O(E^{\frac{1}{2}})$ by setting

$$\frac{\beta L}{2\omega_0} = \beta_0 E^{\frac{1}{2}},$$

where β_0 is assumed of order unity. This assumption is a reasonable one for large scale geophysical motions.

The β-plane analysis is similar to that for the f-plane, i.e. beginning with the dependent variable series expansions of (2.7) one is again led to the governing equations (2.26). In the β-analysis the coefficients following (2.26) are the same as for the f-plane case with the exceptions that a_1 and b_1 are replaced by

$$a_1 = \frac{\beta_0}{kU_1} - \frac{U_2 L \rho_2}{U_1 dS}, \quad b_1 = \frac{\beta_0}{kU_2} - \frac{U_1 L \rho_1}{U_2 (H-d) S}, \tag{3.2}$$

respectively. Because a_1 and b_1 are the coefficients of g_0 and $\tilde{g}_0$ respectively in (2.26)

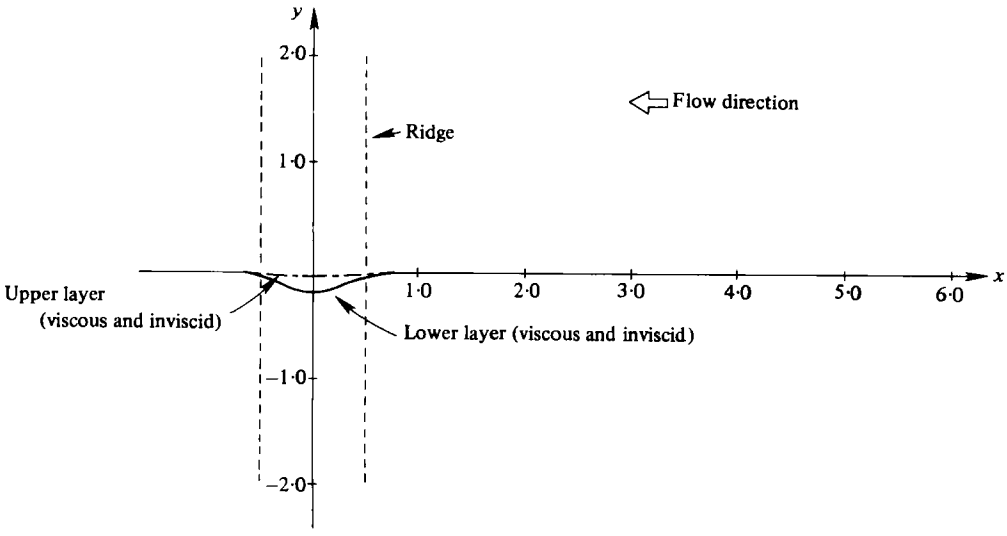

FIGURE 3. Streamline pattern for retrograde (westward) flow over a cosine-squared ridge on a β-plane; $Ro = 0{\cdot}020$, $E = 1{\cdot}94 \times 10^{-4}$, $S = 0{\cdot}48$, $\beta_0 = 9{\cdot}99$ (inviscid), $\beta_0 = 14{\cdot}28$ (viscous), $H/L = 1{\cdot}0$, $d/L = 0{\cdot}5$ and $h/L = 0{\cdot}05$. The free-stream velocity in each layer is the same; i.e. $U_1/U_2 = 1{\cdot}0$. Note, in the inviscid case $E = 0$.

it is then an easy matter to show that given a β and hence a β_0 the first terms on the right-hand sides of (3.2) can be simulated respectively in the laboratory by sloping the lower and upper surfaces in the 'north–south' direction according to

$$(h_{0y})_{\text{lower}} = \beta_0 \frac{d}{L}, \quad (h_{0y})_{\text{upper}} = -\beta_0 \frac{H-d}{L}. \tag{3.3}$$

In summary the viscous β-plane analysis leads to the governing equations (2.26a, b) but with the coefficients a_1 and a_2 in this case being given by

$$a_1 = \frac{(h_{0y})_{\text{lower}} L}{kU_1 d} - \frac{U_2 L \rho_2}{U_1 dS}, \quad b_1 = -\frac{(h_{0y})_{\text{upper}} L}{kU_2(H-d)} - \frac{U_1 L \rho_1}{U_2(H-d)S}. \tag{3.4}$$

The remaining coefficients a_0, a_2, a_3, a_4, b_0, b_2 and b_3 are the same as those following (2.26), respectively. Given β and the upper and lower layer fluid depths, the surface slopes are found from (3.3), where we recall from (2.6) that $h_0(x, y) = h(xL, yL)/(LE^{\frac{1}{2}})$.

The inviscid differential equations for the β-plane case are the same as those for the f-plane (i.e. (2.30)) with the exception that the coefficients a_1 and b_1 are now given by

$$a_1 = \frac{\beta_0}{U_1} - \frac{U_2 L \rho_2}{U_1 dS}, \quad b_1 = \frac{\beta_0}{U_2} - \frac{U_1 L \rho_1}{U_2(H-d)S}, \tag{3.5}$$

respectively, where $\beta_0 = (\beta L)/(2\omega Ro)$ and where the topography function is given by

$$h_0(x, y) = \frac{h(xL, yL)}{LRo}. \tag{3.6}$$

In simulating the β-effect the β_0 term in a_1 and b_1 in relations (3.5) must again be replaced by the relations (3.3) respectively, now using the height function defined in

(3.6). In summary, the inviscid β-analysis leads to the governing equations (2.30) with the coefficients a_1 and b_1 given by

$$a_1 = \frac{(h_{0y})_{\text{lower}} L}{U_1 d} - \frac{U_2 L \rho_2}{U_1 d S}, \quad b_1 = -\frac{(h_{0y})_{\text{upper}} L}{U_2 (H-d)} - \frac{U_1 L \rho_1}{U_2 (H-d) S}, \tag{3.7}$$

respectively, and a_3, a_4 and b_3 given by those relations following (2.30). Given a β and the upper and lower fluid depths, the surface slopes are determined from (3.3) and (3.6). The velocity field is then determined from (2.30) using the coefficients noted above.

Viscous and inviscid solutions for both retrograde (westward) and prograde (eastward) flow were obtained for the cosine squared ridge discussed above using the same parameters as for the f-plane case and in addition taking $\beta = 0{\cdot}079$ cm^{-1} s^{-1}. Solutions for retrograde flow are given in figure 3. The streamline pattern for both the viscous and inviscid cases is confined to small excursions from the uniform flow. Because of the small relative vorticity generated by the topography, viscous effects are relatively unimportant in determining the velocity field; in fact for the parameters considered the streamline patterns are indistinguishable. The observations from figure 3 of relatively small streamline deflections in both layers, with essentially no topographic effect in the upper layer are in consonance with McCartney's (1975) inviscid results for flow past a truncated cylinder.

Solutions for both the viscous and inviscid cases for prograde (eastward) flow are plotted in figure 4. In view of the large relative viscosity generated in both layers by the ridge we note the importance of including viscosity in the analysis. We also note that in the vicinity of the upstream portion of the ridge that the viscous and inviscid solutions are similar. The results, however, diverge dramatically downstream of the ridge. Viscosity damps out the motion within several ridge diameters while in the inviscid case oscillations in the flow established by the ridge continue indefinitely downstream. It is also noted that the streamline pattern in the lower layer is qualitatively similar to that given by Vaziri & Boyer (1977) for prograde flow in a single layer β-plane laboratory experiment. The experimental parameters were similar, but not identical with the values used in the theoretical solution above.

Solutions for an f-plane and β-plane were also obtained for an 'exponential ridge' whose amplitude and cross-sectional area were identical with the cosine-squared ridge above; i.e. the topographic function used was

$$h_0(x) = 3{\cdot}57\, e^{-12{\cdot}57x^2}, \quad -\infty \leqslant x \leqslant \infty,$$

where the horizontal dimension was taken as the width at which the ridge height was 0·043 of the maximum height. The horizontal flow fields so obtained for the same parameters used above were indistinguishable from those results given in figures 2, 3 and 4 for the cosine-squared ridge. Thus the flow field is relatively insensitive to the details of the ridge profile.

The analysis leading to (2.26) is restricted to ridges with continuous slopes. It is noted, however, that solutions were also obtained for topographic features with continuous h_0 but discontinuous h_{0x}; in particular, a ridge of triangular cross-section. In this analysis the height and cross-sectional areas of the triangular ridge were the same as those of the cosine-squared and exponential ridges described above. The horizontal flow patterns for both the f- and β-planes so obtained were again virtually

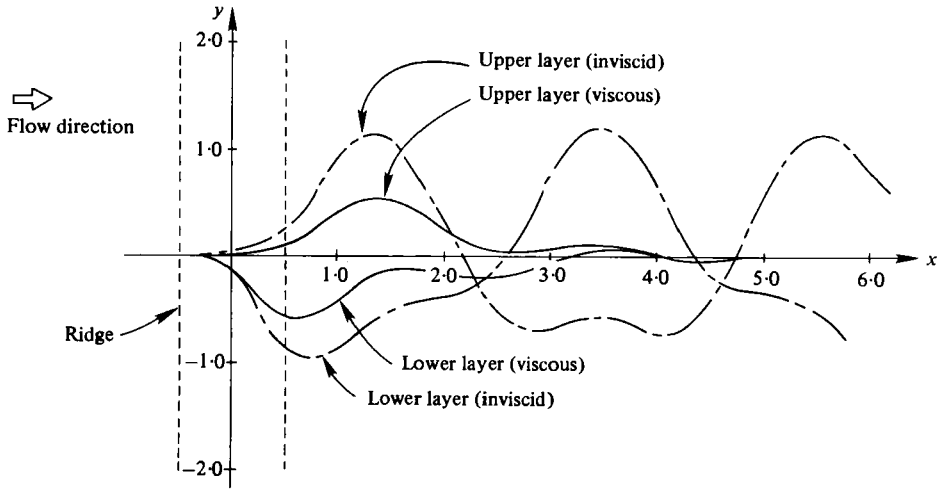

FIGURE 4. Streamline pattern for prograde (eastward) flow over a cosine-squared ridge on a β-plane; $Ro = 0{\cdot}020$, $E = 1{\cdot}94 \times 10^4$, $S = 0{\cdot}48$, $\beta_0 = 14{\cdot}28$ (viscous), $H/L = 1{\cdot}0$, $d/L = 0{\cdot}5$ and $h/L = 0{\cdot}05$. The free-stream velocity in each layer is the same; i.e. $U_1/U_2 = 1{\cdot}0$. Note, in the inviscid case $E = 0$.

identical to those given in figures 2, 3 and 4. So again we find that major features of the flow fields are relatively insensitive to the details of the topographic feature. In addition, it appears the analysis can be extended to a reasonable approximation to features with continuous h_0 but discontinuous h_{0x}.

4. Summary and conclusions

A theory has been developed for both the viscous and inviscid flow of two immiscible fluids over long shallow ridges in a rotating system. In the viscous theory the flow field consists of geostrophic regions in each fluid layer with Ekman boundary layers occurring along the bounding surfaces. The theory also incorporates Ekman layers in each fluid along the interface between the two fluids.

For the f-plane case the inviscid solution shows that downstream of the ridge the streamlines are at an angle to the right, facing downstream, of their upstream directions, a result reminiscent of that given by Batchelor (1970) for a single-layer system. The inclusion of viscosity in the f-plane leads to a flow in which the downstream streamlines are in the same direction as those upstream, but are shifted a finite distance to the right, facing downstream. This latter result is reminiscent, say for the lower layer, of the one-layer experimental results given by Boyer (1971*a*).

In the β-plane analysis it is shown that for a two-layer flow the β-effect can be simulated by appropriately tilting the upper and lower surfaces. For retrograde flow on a β-plane the streamline deflections in both layers are small relative to those for the prograde case. Downstream of the ridge the streamlines return to their upstream positions and directions. Because of the small relative vorticity generated by the ridge, Ekman suction at the bounding surfaces and the interface has little effect on the streamline patterns.

For prograde flow the viscous case leads to large damped oscillatory waves in the

streamline patterns of each layer. The lower-layer solution is qualitatively similar to the single-layer laboratory results conducted by Vaziri & Boyer (1977). The inviscid prograde case leads to large undamped oscillations in the streamline patterns in both layers downstream of the ridge.

The horizontal streamline patterns are found to be relatively insensitive to the details of the ridge shape for ridges with equal amplitude and cross-sectional areas. Furthermore it appears these streamline patterns can be satisfactorily determined for ridges with discontinuous slope even though the theory is strictly valid only for continuous slope cases.

This research was supported by the Ocean Sciences and Technology Division of the Office of Naval Research under Contract no. N00014-76-C-0272 and by the Atmospheric Sciences Division of the National Science Foundation under Grant no. ATM-7905933. The author wishes to thank Dr Abdel-Fatteh Amr, Mr James Ma and Mr Richard Mentock in assisting in solving for the various flow patterns given in this study.

REFERENCES

Batchelor, G. K. 1970 *An Introduction to Fluid Dynamics*. Cambridge University Press.

Boyer, D. L. 1971*a* Rotating flow over long shallow ridges. *Geophysical Fluid Dyn.* **2**, 165–184.

Boyer, D. L. 1971*b* Rotating flow over a step. *J. Fluid Mech.* **50**, 675–687.

Greenspan, H. P. 1968 *The Theory of Rotating Fluids*. Cambridge University Press.

Hide, R. 1961 Origin of Jupiter's Great Red Spot. *Nature* **190**, 895–896.

Huppert, H. E. 1975 Some remarks on the initiation of inertial Taylor columns. *J. Fluid Mech.* **67**, 397–412.

Huppert, H. E. & Stern, M. E. 1974 The effect of side walls on homogeneous rotating flow over two-dimensional obstacles. *J. Fluid Mech.* **62**, 417–436.

McCartney, M. S. 1975 Inertial Taylor columns on a beta plane. *J. Fluid Mech.* **68**, 71–95.

Taylor, G. I. 1923 Experiments on the motion of solid bodies in rotating fluids. *Proc. Roy. Soc.* A **104**, 213–218.

Vaziri, A. & Boyer, D. L. 1971 Rotating flow over shallow topographies. *J. Fluid Mech.* **50**, 79–95.

Vaziri, A. & Boyer, D. L. 1977 Topographically induced Rossby waves. *Arch. Mech.* (*Warszawa*) **29**, 3–12.